

Article

# Fault-Tolerant Control for ROVs Using Control Reallocation and Power Isolation

Romano Capocci <sup>1,\*</sup>, Edin Omerdic <sup>1</sup>, Gerard Dooly <sup>1</sup> and Daniel Toal <sup>1</sup>

<sup>1</sup> CRIS – Centre for Robotics & Intelligent Systems, University of Limerick, Castletroy, Limerick V94 T9PX, Ireland. edin.omerdic@ul.ie (E.O.); gerard.dooly@ul.ie (G.D.); daniel.toal@ul.ie (D.T.)

\* Correspondence: romano.capocci@ul.ie (R.C.); Tel.: +353-(0)85-759-3011

**Abstract:** This paper describes a novel thruster fault-tolerant control system (FTC) for open-frame remotely operated vehicles (ROVs). The proposed FTC consists of two subsystems: a model-free thruster fault detection and isolation subsystem (FDI) and a fault accommodation subsystem (FA). The FDI subsystem employs fault detection units (FDUs), associated with each thruster, to monitor their state. The robust, reliable and adaptive FDUs use a model-free pattern recognition neural network (PRNN) to detect internal and external faulty states of the thrusters in real time. The FA subsystem combines information provided by the FDI subsystem with predefined, user-configurable actions to accommodate partial and total faults and to perform an appropriate control reallocation. Software-level actions include penalisation of faulty thrusters in solution of control allocation problem and reallocation of control energy among the operable thrusters. Hardware-level actions include power isolation of faulty thrusters (total faults only) such that the entire ROV power system is not compromised. The proposed FTC system is implemented as a LabVIEW virtual instrument (VI) and evaluated in virtual (simulated) and real-world environments. The proposed FTC module can be used for open frame ROVs with up to 12 thrusters: eight horizontal thrusters configured in two horizontal layers of four thrusters each, and four vertical thrusters configured in one vertical layer. Results from both environments show that the ROV control system, enhanced with the FDI and FA subsystems, is capable of maintaining full 6 DOF control of ROV in the presence of up to 6 simultaneous total faults in the thrusters. With the FDI and FA subsystems in place the control energy distribution of the healthy thrusters is optimised so that the ROV can still operate in difficult conditions under fault scenarios.

**Keywords:** fault-tolerant control; thruster fault; fault detection and isolation; fault accommodation; ROV; remotely operated vehicle; underwater vehicle;

## 1. Introduction

Over the past decades, the use of ROVs has become more widespread. This is due to the reduction in costs driven by military and oil and gas research, making the technology available for other commercial and scientific purposes [1]. In more recent years ROVs have been employed for survey contracts and, with the push in the marine renewable energy (MRE) sector, ROVs will need to be capable of operating in more difficult environments to carry out close quarters inspections of the MRE devices and structures, thus reducing operational costs within the sector. The environment in which ROVs operate can be unpredictable, with the external parts of the system being subjected to seawater, changes in temperature, high pressures and interactions with solids drifting through the water column. These factors all contribute toward possibilities of thrusters becoming damaged or developing faults in their dynamic parts. In the past, it was common to abort a mission if a fault occurred in a thruster. Due to reduced weather windows at the sites of MRE converters [2], the expensive nature of ROV operations and the drive to reduce costs this method should be avoided, if possible. FTC within ROVs can be utilised to combat this. Due to the particular advantages of FTC in ROV applications, many different techniques have been proposed. One recent approach monitored the thruster voltage and current and, if a fault was detected, utilised a fuzzy method to accommodate the faults in the control of the ROV [3]. The FTC system for an ROV, proposed in [4],

used a modified version of the Moore-Penrose pseudo inverse to redistribute the control effort to healthy thrusters if a fault occurs.

In the literature the majority of the fault-tolerant control methods proposed for underwater vehicles have been integrated and evaluated in a simulated environment [5-9]. As a first step for evaluation this approach is beneficial but, when practical and affordable, real-world trials should be conducted to evaluate the system in the environment in which it is expected to operate. Real-world trials have been conducted in some cases to evaluate the FTC of the ROV [10,11], generating more accurate results.

This paper presents an active fault-tolerant control system for an ROV using a combination of thruster fault detection and isolation, faulty thruster power isolation and fault accommodation in the control of the ROV. The word "active" means that the method is based on active monitoring of relevant signals from the thrusters (currents, shaft speeds, applied voltages and temperatures of windings). For thrusters that cannot provide these signals, the authors are currently working on novel "passive" method for fault detection and isolation. It is expected to publish the main features of the "passive" method and comparison table of both methods in Spring 2018.

Most underwater vehicle fault detection schemes are model-based, and concern the dynamic relationship between actuators and vehicle behaviour or the specific input-output thruster dynamics [3]. The proposed thruster FDI approach is a model-free scheme based on a pattern recognition neural network, trained with simulated and real-world data. New features of the proposed FTC includes separation of the virtual control space into vertical and horizontal thruster subspaces (planes) and real-world implementation in the real-time ROV control system for various thruster configurations. The thruster FA subsystem receives thruster state data from the FDI and, in the case of a fault, reallocates thruster forces by reducing the saturation bounds of the faulty thruster (software-level action A). At the same time, in case of total faults, the thruster power is switched off (hardware-level action B), in order to prevent a threat to full power system and reduce the risk of damage to other ROV components.

The proposed FTC system has been successfully tested in a virtual environment (using a real time ROV simulator) and a real world environment (using VideoRay M5 thrusters) in a test tank at the University of Limerick (UL). The proposed FTC system is part of the OceanRINGS+ ROV smart control system, currently under development at CRIS, UL.

The paper outline is provided as follows. In section 2 background information is provided, including links with other research projects and a short description of Inspection ROV (IROV). The architecture of the FTC, including description and implementation of the FDI & FA subsystems, is described in section 3. Section 4 presents the testing and evaluation results of the proposed FTC in real-world and virtual (simulated) environments. Finally, concluding remarks and directions for future work are provided in section 5.

## 2. Background

### 2.1. OceanRINGS+

OceanRINGS is an Internet/Ethernet-enabled ROV control system, based on robust control algorithms, deterministic network-oriented hardware and flexible, 3-layer software architecture [12]. ROV LATIS is a prototype platform developed at UL to test and validate OceanRINGS [13]. System validation and technology demonstration has been performed over the last eight years through a series of test trials with different support vessels. Operations include subsea cable inspection/survey, wave energy farm cable to shore routing, shipwreck survey, ROV-ship synchronisation and oil spill/HNS incident response.

Currently, researchers at UL are developing the next generation of the ROV control system (OceanRINGS+, the extended version of OceanRINGS). The highly adaptive 3-layer software architecture of OceanRINGS+ includes fault-tolerant control allocation algorithms in the bottom layer, transparent interface between an ROV and supporting platforms (surface platforms, surface/subsea garages and/or supporting vessels) in the middle layer and assistive tools for mission execution/monitoring/supervision in the top layer. Software modules have been developed for

advanced control modes, such as auto compensation of ocean currents based on ROV absolute motion, robust speed/course controller with independent heading control, semi and full auto pilot capabilities, auto-tuning procedure for low-level controllers, ROV high precision dynamic position & motion control in absolute earth-fixed frame, or relative to target or support platform/vessel. This paper is focused on the description of the FTC, the module at the bottom layer of the full OceanRINGS<sup>+</sup> control architecture.

2.2. Inspection ROV (IROV)

As part of the ongoing MaREI research project “Smart Inspection ROVs for Use in Challenging Conditions”, researchers at the Centre for Robotics & Intelligent Systems (CRIS), University of Limerick have designed and developed a reconfigurable, inspection-class ROV (IROV) in the period of 2014-2018, aimed to perform periodic and post storm inspection of offshore MRE converters, moorings and foundations, reducing the need for commercial divers to be employed in this difficult and potentially dangerous environment. The IROV (Figure 1) is a reconfigurable system with the option to utilise two types of thrusters in different configurations.



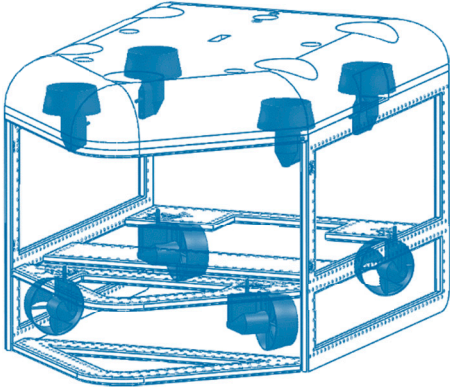
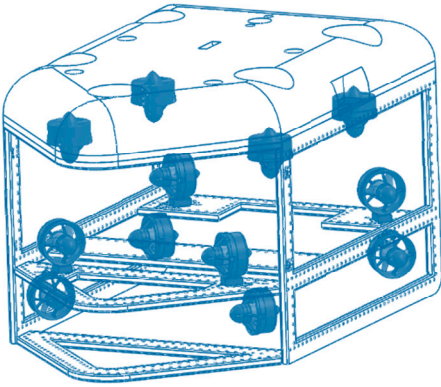
Figure 1. Observation class IROV, developed by CRIS researchers, UL.

The reconfigurable propulsion system of IROV includes two thruster configurations (Table 1):

- **Configuration 1:** Eight VideoRay M5 thrusters configured in two layers: Horizontal Layer with four thrusters and Vertical Layer with four thrusters. These thrusters provide active monitoring of relevant signals from thrusters (currents, shaft speeds, applied voltages and temperatures of windings).
- **Configuration 2:** Twelve BlueRobotics T200 thrusters configured in three layers: Horizontal Layers L0 and L1 with four thrusters each and Vertical Layer with four thrusters. These thrusters cannot provide monitoring of relevant signals and the passive FTC system for this class of thruster is under development.

125

**Table 1.** Thruster configurations.

Configuration 1: 8 x M5 Thrusters	Configuration 2: 12 x T200 Thrusters
	
Horizontal Layer: HT1, HT2, HT3, HT4	Horizontal Layer (L0): HT1, HT2, HT3, HT4
	Horizontal Layer (L1): HT1, HT2, HT3, HT4
Vertical Layer: VT1, VT2, VT3, VT4	Vertical Layer: VT1, VT2, VT3, VT4

126  
127  
128  
129  
130  
131  
132  
133  
134

It should be emphasized that the OceanRINGS+ control architecture has been designed to be generic, i.e. not limited to exclusive use by IROV, but any ROV with standard physical layout of thrusters. Although testing and validation of proposed FTC is performed with IROV configured as Configuration 1, the active FTC proposed in this paper and implemented as part of OceanRINGS+ is applicable to open-frame ROVs with a maximum of 12 thrusters subject to the constraint that each thruster can provide measurement of relevant signals (currents, shaft speeds, applied voltages and temperatures of windings). The FDI subsystem detects faults in thrusters regardless of their physical layout. However, for successful fault accommodation, the physical layout of thrusters plays an important role.

135 **3. Fault-Tolerant Control (FTC) System**

136 *3.1. FTC architecture*

137  
138  
139  
140  
141  
142  
143  
144  
145  
146  
147  
148  
149  
150  
151  
152  
153  
154  
155  
156  
157

The overall functional architecture of the proposed FTC system is shown in Figure 2. The description of the architecture is provided in a hierarchical manner, such that the general description and the main idea are introduced first, while more details about individual components can be found in the following subsections. This architecture is an extension of the control architecture proposed in [14].

In contrast to the Fault Diagnosis and Accommodation System (FDAS), proposed in [15] and implemented in the original version of OceanRINGS, there are a number of new features in the FTC architecture shown in Figure 2 and implemented in OceanRINGS+. Firstly, there is a clear separation between horizontal and vertical thrusters using decomposition of motion into horizontal and vertical subspaces (planes). Secondly, there is provision for two layers of horizontal thrusters and one layer of vertical thrusters. Thirdly, the Fault Detection Units utilize a pattern recognition neural network for real-time fault detection instead of self-organising maps.

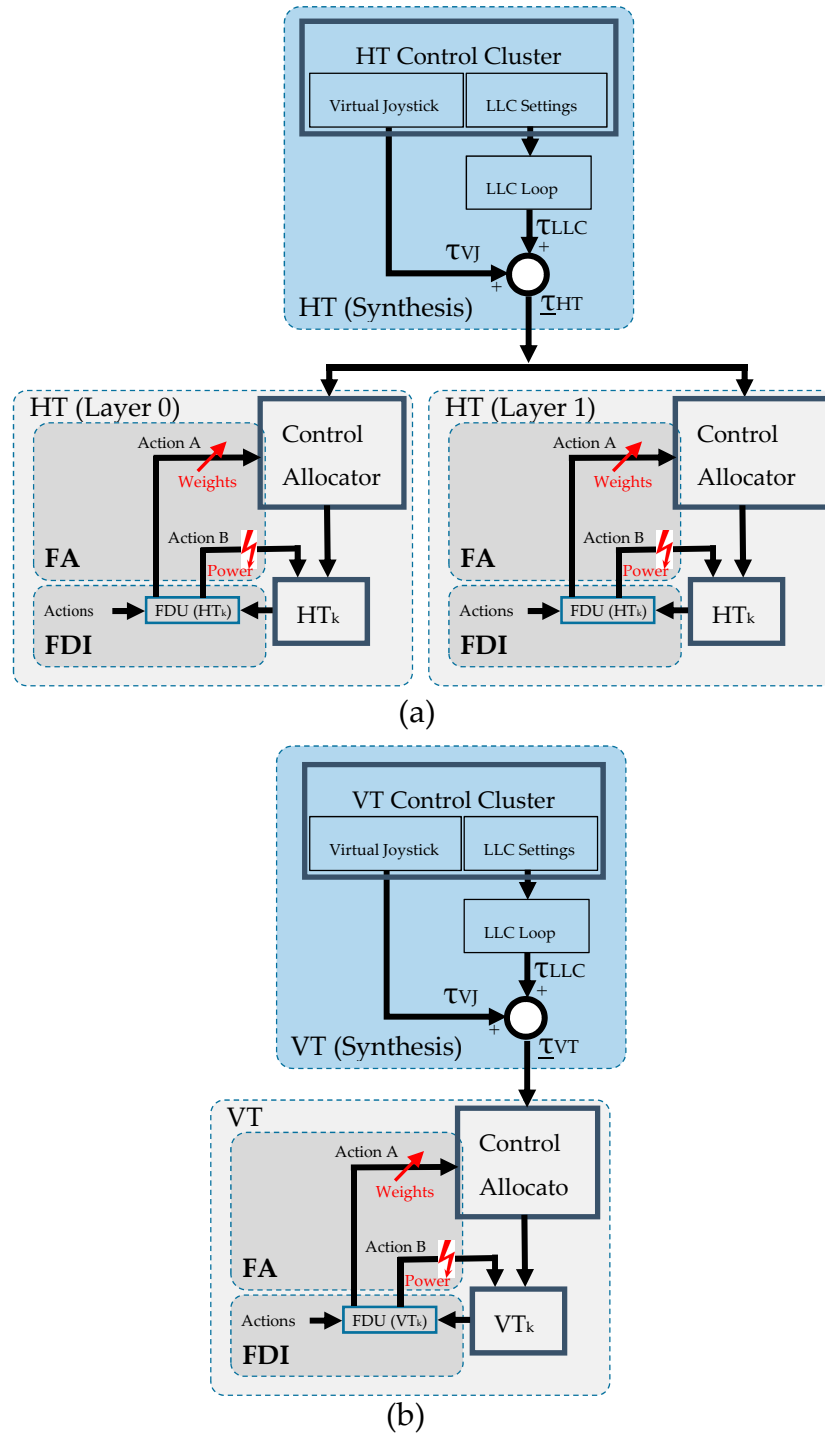


**Figure 2.** Architecture of the Fault Tolerant Control (FTC) system: (a) Horizontal Subspace (Plane); (b) Vertical Subspace (Plane).

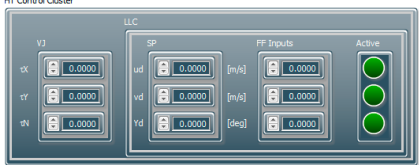
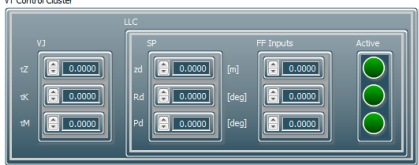
The virtual control input  $\tau$  for the control allocation is a normalised vector of forces and moments:  $\tau = [\tau_X \ \tau_Y \ \tau_Z \ \tau_K \ \tau_M \ \tau_N]^T$ , where  $\tau_X$  is surge force,  $\tau_Y$  is sway force,  $\tau_Z$  is heave force,  $\tau_K$  is roll moment,  $\tau_M$  is pitch moment, and  $\tau_N$  is yaw moment. Decomposition of this vector into the horizontal and vertical planes is presented in Table 2.

The Control Clusters (Figure 2 and Table 2) are links between the FTC module in the bottom layer and upper layers in control architecture. The HT Control Cluster consists of two subclusters: Virtual Joystick (to mimic direct surge & sway forces and yaw moment generated by human or virtual pilot) and a set of settings for Low-Level Controllers (set points for surge speed  $u_d$  (m/s), sway speed  $v_d$  (m/s) and heading  $Y_d$  (°), feed-forward inputs and on/off switches to enable/disable



individual controllers). The VT Control Cluster has two subclusters: Virtual Joystick (to mimic direct heave force and roll & pitch moments generated by human or virtual pilot) and a set of settings for Low-Level Controllers (set points for depth/altitude  $z_d$  (m), roll  $R_d$  (°) and pitch  $P_d$  (°), feed-forward inputs and on/off switches to enable/disable individual controllers). Inside the Synthesis module the LLC Settings subclusters are used as one of the inputs to the LLC loops (the other inputs are navigation data and parameters of controllers). There is a single controller for each degree of freedom (DOF). Surge and Sway controllers are velocity controllers, while Heave, Roll, Pitch & Yaw are position controllers. Further information about the internal structure of LLC loops can be found in [16]. Individual outputs of LLC loops are bundled into vectors  $\tau_{LLC}$ . The final outputs of the Synthesis module are vectors  $\tau_{HT}$  and  $\tau_{VT}$ , obtained by summation and normalisation of corresponding vectors  $\tau_{VJ}$  and  $\tau_{LLC}$  for each subspace, respectively.

**Table 2.** Decomposition into Horizontal and Vertical Subspaces (Planes).

Virtual Control Input	Horizontal Plane $\tau_{HT}$	Vertical Plane $\tau_{VT}$
$\tau = \begin{bmatrix} \tau_X \\ \tau_Y \\ \tau_Z \\ \tau_K \\ \tau_M \\ \tau_N \end{bmatrix}$	$\tau_{HT} = \begin{bmatrix} \tau_X \\ \tau_Y \\ \tau_N \end{bmatrix}$ <div><math>\tau_X</math> – Surge Force <math>\tau_Y</math> – Sway Force <math>\tau_N</math> – Yaw Moment</div> <div></div>	$\tau_{VT} = \begin{bmatrix} \tau_Z \\ \tau_K \\ \tau_M \end{bmatrix}$ <div><math>\tau_Z</math> – Heave Force <math>\tau_K</math> – Roll Moment <math>\tau_M</math> – Pitch Moment</div> <div></div>

Each layer of horizontal thrusters has its own FDI, FA and Control Allocator module. It should be emphasized that both layers of horizontal thrusters are independent from each other, i.e. they can have a different physical layout and number of thrusters. In the Horizontal Plane, both layers have the same input (vector  $\tau_{HT}$ ), which is the output of HT Synthesis module.

3.2. FDI subsystem

**Fault Classification:** Thrusters are liable to different fault types during the underwater mission e.g. propellers can be jammed, broken or lost, water can penetrate inside the thruster enclosure, communication between the thruster and the master node can be lost, applied voltage or temperature of the winding can exceed the threshold, etc. Some of these faults (partial faults) are not critical and the thruster is able to continue operation in the presence of a fault with the restricted usage, i.e. reduced maximum velocity. In other cases (total faults – failures) the thruster must be switched off and the mission has to be continued with remaining operable thrusters. Thruster faults are classified into two main classes:

- *Internal faults* (e.g. temperature of the windings is out of range, drop in bus voltage etc.),
- *External faults* (e.g. lightly jammed, jammed, heavily jammed, lost or broken propeller).

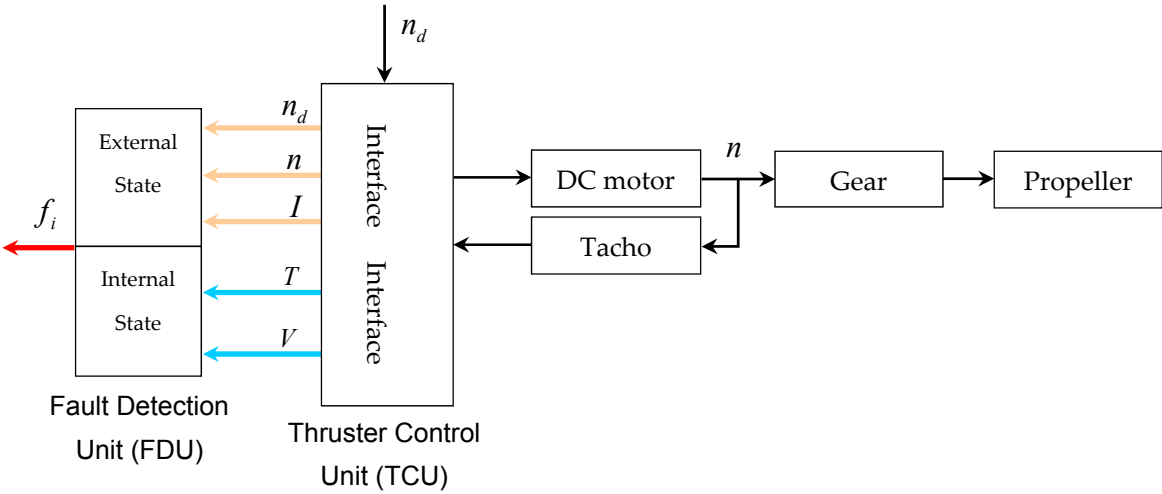
**Fault Code Table:** Relationships between thruster states, fault types and remedial actions are stored in the thruster fault code table (Table 3). It must be emphasized, at this point, that this fault code table is just a suggestion, intended to reveal the main ideas of the proposed FTC system. New states (rows) can be added, and the existing relationships can be changed, in order to accommodate specific requirements and available thruster data.

247

Table 3. Thruster Fault Code Table.

Thruster State	Class	Type	Action A: Saturation Bounds	Action B: Thruster Power
Invalid	-	-	1.00	ON
Healthy	-	-	1.00	ON
Lightly Jammed	External	Partial	0.75	ON
Jammed	External	Partial	0.25	ON
Heavily Jammed	External	Total	0.00	OFF
Broken Propeller	External	Total	0.00	OFF
Unknown	External	Total	0.00	OFF
Voltage outside threshold	Internal	Total	0.00	OFF
Temp. outside threshold	Internal	Total	0.00	OFF

248       **Fault Detection Unit (FDU):** It is assumed that each thruster is driven by a Thruster Control  
249 Unit (TCU), with integrated power amplifiers and a microcontroller (Figure 3). The input to the TCU  
250 is desired shaft speed  $n_d$  (%). The outputs are current  $I$  (A), shaft speed  $n$  (rpm), bus voltage  $V$   
251 (V) and temperature  $T$  (°C) of windings. The outputs of each thruster are sent to the associated FDI  
252 module in real-time. The FDI module utilises the Fault Detection Units (FDUs) to monitor the state  
253 of the thrusters. The FDU is a software module associated with the thruster, able to detect internal  
254 faults and external faults. The output of the FDU is a fault state vector  $f_i$ . Connections between the  
255 FDU and the TCU for an arbitrary thruster  $T_i$  are indicated in Figure 3.



256

257       **Figure 3.** Block diagram showing connections between the FDU and the TCU for thruster  $T_i$ .

258       Signals for detection of internal faults are already available in existing TCUs for VideoRay  
259 thrusters M5. In particular, the communication protocol for the M5 provides monitoring of the  
260 winding temperature  $T$  (°C) and bus voltage  $V$  (V) of each thruster. In order to build a universal  
261 FDU, able to detect both internal and external faults, it is necessary to augment the existing internal  
262 protection with a software module for fast and reliable detection of external faults.

263       For detection of external faults available signals are desired: shaft speed  $n_d$  (%), actual shaft  
264 speed  $n$  (rpm) and current consumption  $I$  (A) of the thruster. By monitoring  $n$  and  $I$ , together  
265 with desired shaft speed  $n_d$ , obtained as the output of the Control Allocation, the FDU is designed  
266 to detect, isolate and categorise external thruster faults using Pattern Recognition Neural Network  
267 (PRNN).

268       Finally, the universal FDU integrates both parts (internal and external) into one unit, which is  
269 able to detect both internal and external faults (Figure 3). Integration includes a priority scheme,  
270 where total faults have higher priority than partial faults. The fault state vector  $f_i$ , the output of the  
271 FDU, is the code of the fault.

**Implementation:** Implementation involves two phases: *off-line training* and *on-line fault detection*.

Off-line training phase

The *first stage* in the training phase is acquisition of training data. In the virtual environment, thruster faults are simulated by varying properties of the thruster dynamic model (load, friction, etc.) inside the propulsion subsystem of the ROV dynamics simulator. In the real-world environment, various jammed propeller faults are simulated such that the objects of different sizes, shapes and weights were attached to the blades, while a broken propeller was simulated with all blades removed from the shaft.

Further details about acquisition of training data in real-world environment is given in the following. A normal state and four different fault cases were considered (lightly jammed, jammed, heavily jammed and broken (lost) propeller). A test rig has been set up and thruster mounted in a test tank in the University of Limerick. To mimic the jammed thruster states various objects (“blockages”) have been attached to the thruster propeller during tests. The thruster test setup and “blockages” are shown in Figure 4. Each “blockage” reduces efficiency of the thruster due to increased load on the shaft and reduced flow of the water through the duct.

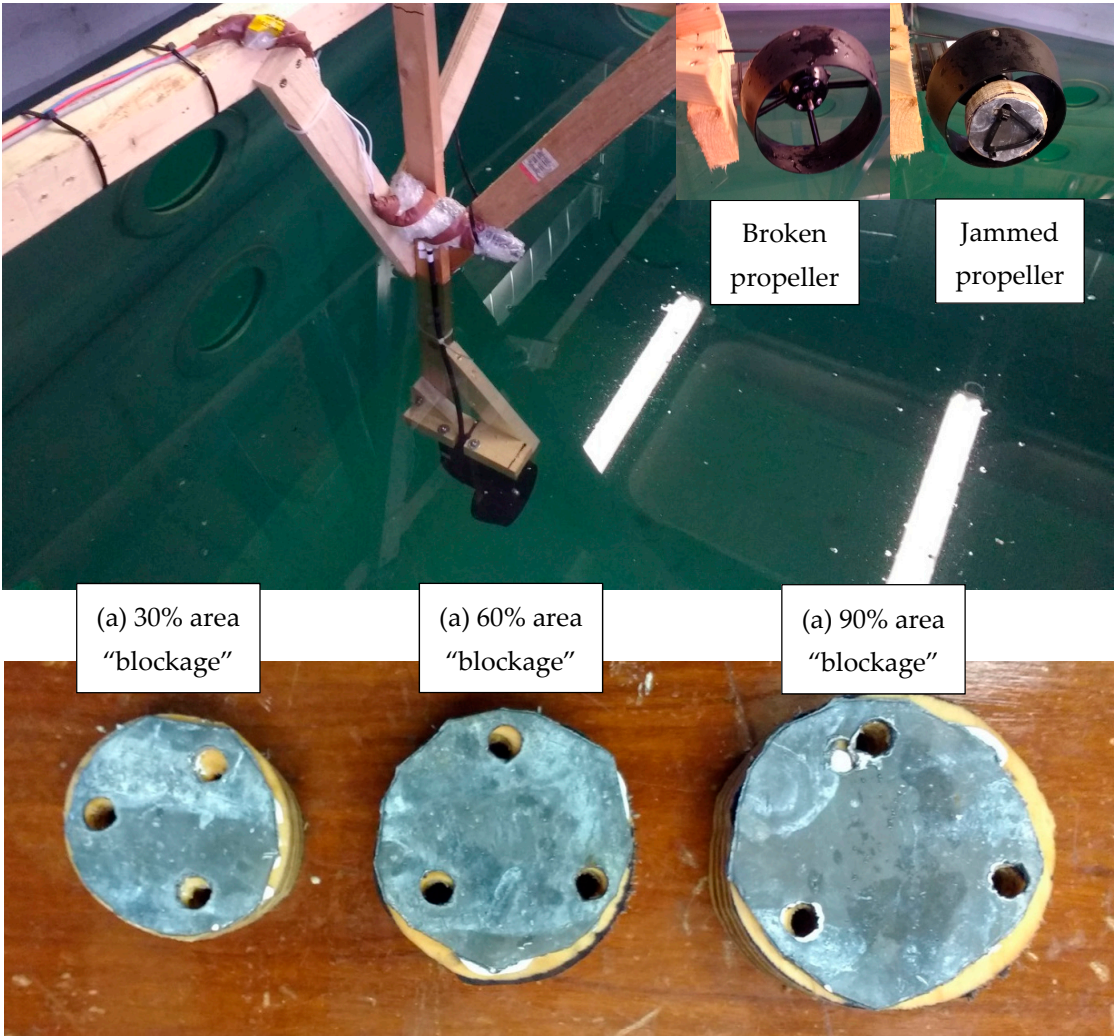


**Figure 4.** Thruster setup for acquisition of real-world data: (a) 30% area “blockage”; (b) 60% area “blockage”; (c) 90% area “blockage”.



291

**Table 4.** Thruster states & setup for real-world data acquisition.

Thruster State	Setup
Healthy	No blockage
Lightly Jammed	Blockage (30% area)
Jammed	Blockage (60% area)
Heavily Jammed	Blockage (90% area)
Broken Propeller	Propeller detached

292

The relationship between the thruster states and setup for real-world data acquisition is given in Table 4. For each state in Table 4, the thruster was actuated with a saw-like command signal  $n_d$  (%) with the following pattern:  $0\% \gg MAX\% \gg 0\% \gg -MAX\% \gg 0\%$ , with a step size 1%. The total duration of signal was 20 seconds, sampling period 50 ms and max. value  $MAX = 100\%$ . In each iteration the desired shaft speed  $n_d$  (%), actual shaft speed  $n$  (rpm) and current consumption  $I$  (A) have been logged. The real-world raw data acquired for each thruster state are presented in Figure 5.

298

Analysing the distribution of the training data in Figure 5, the *first* feature that can be noticed is that each fault type creates a certain pattern. The presence of measurement noise is noticeable in acquired data for currents, resulting in patterns which exhibit a fuzzy (“cloudy”) look. The *second* feature is that it is very difficult to distinguish individual patterns in the zone around  $n_d \approx 0$  (called the *critical zone*). This makes successful fault detection and isolation in the critical zone difficult to achieve. In particular, for the near-zero velocity case  $n_d \approx 0$  the thruster does not rotate or rotates very slowly, reliable fault detection is impossible. The solution to this issue is the exclusion of the critical zone from FDI during the on-line fault detection phase. For this reason, the critical zone is called the *forbidden* zone with associated “Invalid” thruster state. When desired shaft speed is in this zone, the FDI algorithm goes to sleep mode and outputs the “Invalid” state without any action.

308

Each fault type in Figure 5 is characterised by specific features, which makes them different from the other types. These features are discussed in the following. In general, all the variables ( $n_d$ ,  $I$  and  $n$ ) are correlated, i.e. they tend to rise and fall together in a non-linear way. For lightly jammed, jammed and heavily jammed propeller states, objects (“blockages”) attached to the blades generate an additional load for the motor, leading to higher current  $I$  and lower  $n$  than in the fault-free case for the same value of  $n_d$ . In the case of a broken propeller, the absence of the blades means that the load for the motor is much smaller than in other cases, yielding a reduction in current consumption and a significant increase in shaft speed. However, the thruster does not generate any propulsion force in this case.

316

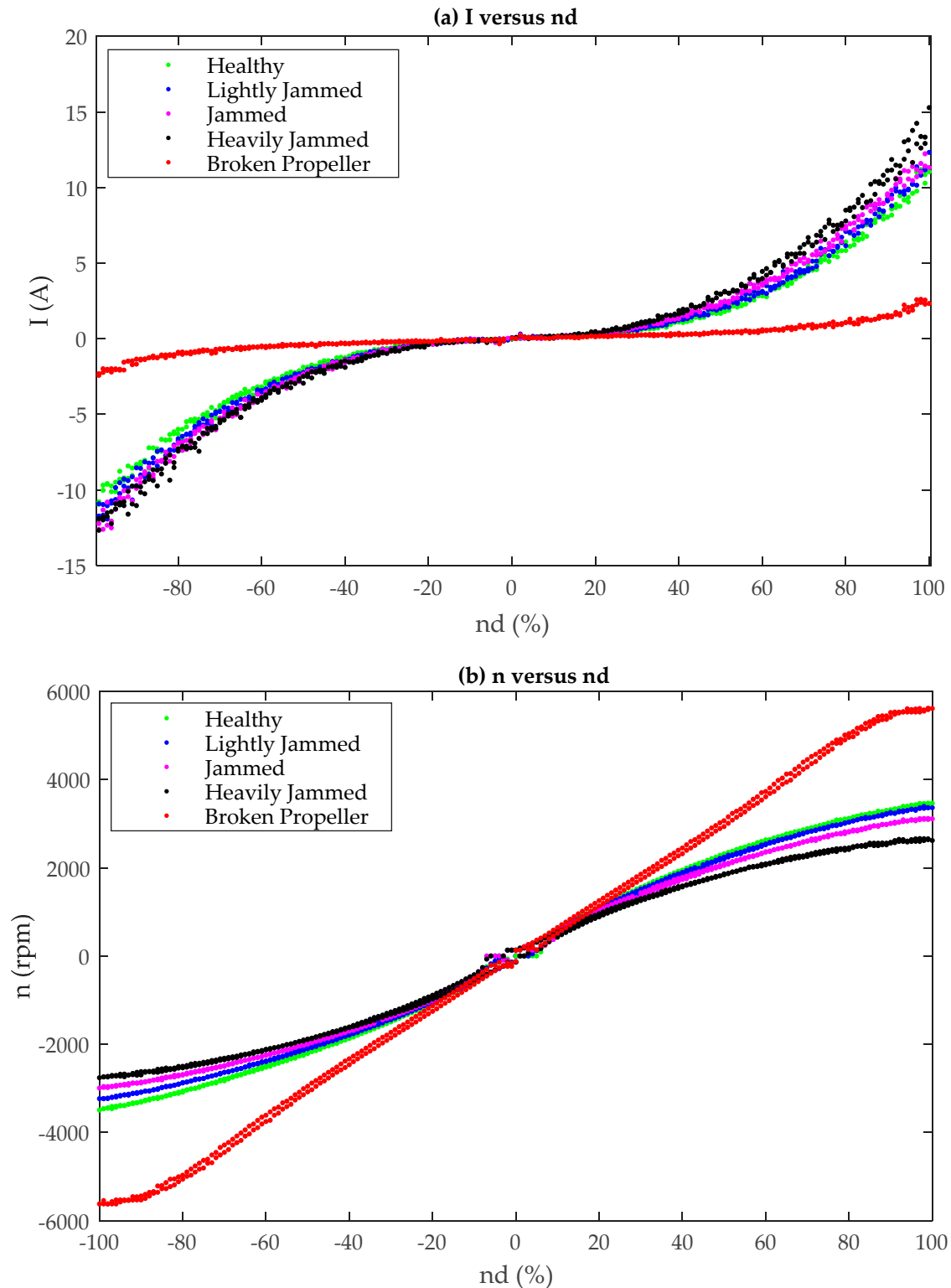


**Figure 5.** Time diagrams of raw training data: (a):  $I$  versus  $n_d$  plot; (b)  $n$  versus  $n_d$  plot.

The main idea of the *second stage* in the training phase is to use the acquired data from the first stage to train a Pattern Recognition Neural Network (PRNN). In order to improve the PRNN classification accuracy, the raw data shown in Figure 5 have been first replaced with best fit curves, as shown in Figures 6 & 7, before creating input-output data sets for NN training. The MATLAB App "Curve Fitting" has been employed to generate best fit curves. Details of the Curve Fitting functions and their parameters can be found in Table 5.

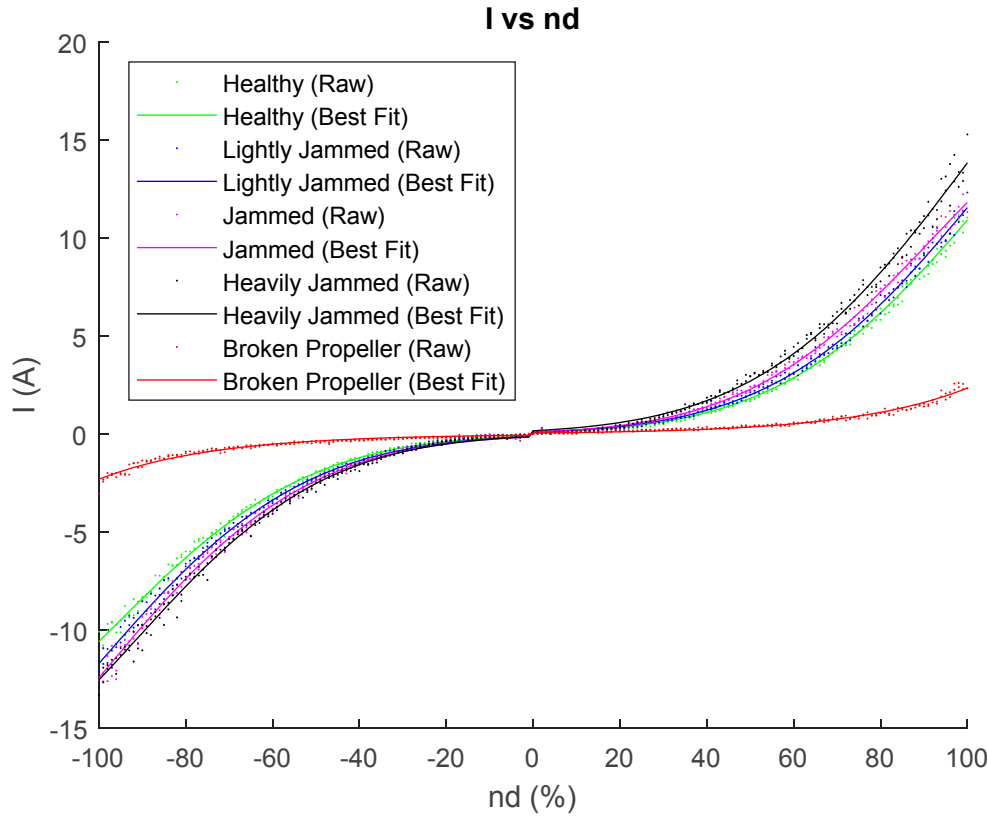


Figure 6. Time diagrams of raw & best fit training data:  $I$  versus  $n_d$  plot.

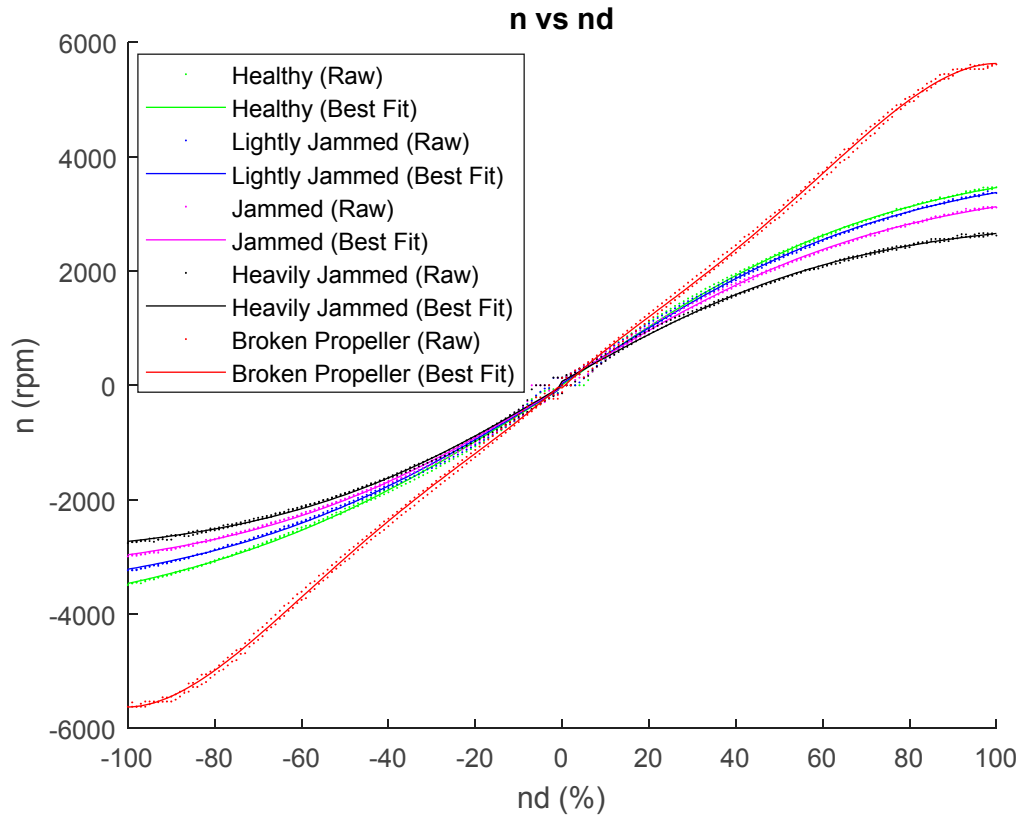


Figure 7. Time diagrams of raw & best fit training data:  $n$  versus  $n_d$  plot.

Table 5. Curve Fitting functions for thruster states.

Thruster State Dataset Plot	Curve Fitting Function Type	Curve Fitting Function	Coefficients
Healthy nd v I <i>positive</i>	Gaussian	$f(x) = a \cdot \exp(-((x-b)/c)^2)$	$a = 19.15, b = 147.8, c = 63.78$
Healthy nd v I <i>negative</i>	Gaussian	$f(x) = a \cdot \exp(-((x-b)/c)^2)$	$a = -16.07, b = -140.2, c = 62.24$
Healthy nd v n <i>positive</i>	Hyperbolic tangent	$f(x) = a \cdot \tanh(b \cdot x) + c$	$a = 4008, b = 0.01298, c = 7.086$
Healthy nd v n <i>negative</i>	Hyperbolic tangent	$f(x) = a \cdot \tanh(b \cdot x) + c$	$a = 4212, b = 0.01134, c = -42.63$
Lightly Jammed nd v I <i>positive</i>	Gaussian	$f(x) = a \cdot \exp(-((x-b)/c)^2)$	$a = 20.04, b = 147.8, c = 64.41$
Lightly Jammed nd v I <i>negative</i>	Gaussian	$f(x) = a \cdot \exp(-((x-b)/c)^2)$	$a = -19.26, b = -145.9, c = 65.05$
Lightly Jammed nd v n <i>positive</i>	Hyperbolic tangent	$f(x) = a \cdot \tanh(b \cdot x) + c$	$a = 3908, b = 0.01274, c = 30.12$
Lightly Jammed nd v n <i>negative</i>	Hyperbolic tangent	$f(x) = a \cdot \tanh(b \cdot x) + c$	$a = 3764, b = 0.01237, c = -37.82$
Jammed nd v I <i>positive</i>	Gaussian	$f(x) = a \cdot \exp(-((x-b)/c)^2)$	$a = 16.27, b = 133.9, c = 59.91$
Jammed nd v I <i>negative</i>	Gaussian	$f(x) = a \cdot \exp(-((x-b)/c)^2)$	$a = -20.4, b = -146.1, c = -65.54$
Jammed nd v n <i>positive</i>	Hyperbolic tangent	$f(x) = a \cdot \tanh(b \cdot x) + c$	$a = 3565, b = 0.01289, c = 60.38$
Jammed nd v n <i>negative</i>	Hyperbolic tangent	$f(x) = a \cdot \tanh(b \cdot x) + c$	$a = 3352, b = 0.01355, c = -29.18$
Heavily Jammed nd v I <i>positive</i>	Gaussian	$f(x) = a \cdot \exp(-((x-b)/c)^2)$	$a = 22.92, b = 147.3, c = 66.57$
Heavily Jammed nd v I <i>negative</i>	Gaussian	$f(x) = a \cdot \exp(-((x-b)/c)^2)$	$a = -17.17, b = -134, c = 60.65$
Heavily Jammed nd v n <i>positive</i>	Hyperbolic tangent	$f(x) = a \cdot \tanh(b \cdot x) + c$	$a = 2875, b = 0.01468, c = 68.49$
Heavily Jammed nd v n <i>negative</i>	Hyperbolic tangent	$f(x) = a \cdot \tanh(b \cdot x) + c$	$a = 3007, b = 0.01488, c = -14.55$
Broken Propeller nd v I <i>positive</i>	Exponential	$f(x) = a \cdot \exp(b \cdot x)$	$a = 0.05542, b = 0.03747$
Broken Propeller nd v I <i>negative</i>	Exponential	$f(x) = a \cdot \exp(b \cdot x)$	$a = -0.05494, b = -0.03735$
Broken Propeller nd v n <i>positive</i>	Polynomial	$f(x) = p_1 \cdot x^4 + p_2 \cdot x^3 + p_3 \cdot x^2 + p_4 \cdot x + p_5$	$p_1 = -0.0001074, p_2 = 0.01742, p_3 = -0.8264, p_4 = 72.56, p_5 = -46.07$
Broken Propeller nd v n <i>negative</i>	Polynomial	$f(x) = p_1 \cdot x^4 + p_2 \cdot x^3 + p_3 \cdot x^2 + p_4 \cdot x + p_5$	$p_1 = 0.0001022, p_2 = 0.0163, p_3 = 0.7478, p_4 = 70.58, p_5 = 34.14$



A two-layer feed-forward network, with 16 sigmoid hidden and 5 softmax output neurons has been trained to classify input vectors. The architecture of the Pattern Recognition Neural Network is shown in Figure 8.

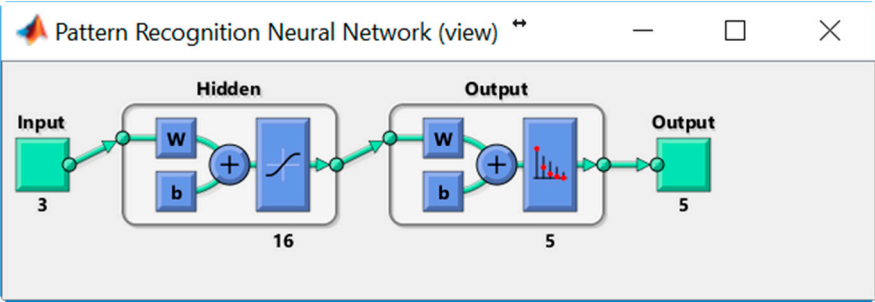


Figure 8. The architecture of Pattern Recognition Neural Network.

As indicated in Table 4, there are five classes (Healthy, Lightly Jammed, Jammed, Heavily Jammed and Broken Propeller). The input data set (matrix **thrusterInputs\_RWE**) has dimension  $3 \times 1005$  and consists of five Input Blocks: **thrusterInputs0\_RWE**, **thrusterInputs1\_RWE**, ..., **thrusterInputs4\_RWE** (one block for each class, see Table 6). Network inputs are stored in columns of the matrix **thrusterInputs\_RWE**. For each class, values of  $n_d$  are -100, -99, ..., +99, +100.

Table 6. Structure of the input training data set **thrusterInputs\_RWE**.

Class	Input Block	Size	Column(j)
Healthy	<b>thrusterInputs0_RWE</b>	$3 \times 201$	$n_d(j); I(j); n(j)$
Lightly Jammed	<b>thrusterInputs1_RWE</b>	$3 \times 201$	$n_d(j); I(j); n(j)$
Jammed	<b>thrusterInputs2_RWE</b>	$3 \times 201$	$n_d(j); I(j); n(j)$
Heavily Jammed	<b>thrusterInputs3_RWE</b>	$3 \times 201$	$n_d(j); I(j); n(j)$
Broken Propeller	<b>thrusterInputs4_RWE</b>	$3 \times 201$	$n_d(j); I(j); n(j)$

The target data set (matrix **thrusterTargets\_RWE**) has dimension  $5 \times 1005$  and consists of five Target Blocks: **thrusterTargets0\_RWE**, **thrusterTargets1\_RWE**, ..., **thrusterTargets4\_RWE** (one block for each class, see Table 7). For class  $k$  columns of corresponding Target Block have 1 at position  $k$ , while all other column elements have value 0.

Table 7. Structure of the output training data set **thrusterTargets\_RWE**.

Class	Target Block	Size	Column
Healthy	<b>thrusterTargets0_RWE</b>	$5 \times 201$	1; 0; 0; 0; 0
Lightly Jammed	<b>thrusterTargets1_RWE</b>	$5 \times 201$	0; 1; 0; 0; 0
Jammed	<b>thrusterTargets2_RWE</b>	$5 \times 201$	0; 0; 1; 0; 0
Heavily Jammed	<b>thrusterTargets3_RWE</b>	$5 \times 201$	0; 0; 0; 1; 0
Broken Propeller	<b>thrusterTargets4_RWE</b>	$5 \times 201$	0; 0; 0; 0; 1

Algorithms used in PRNN training are provided in Table 8.

Table 8. Pattern Recognition Neural Network training algorithms.

Algorithms	
Data Division	Random (dividerand)
Training	Scaled Conjugate Gradient (trainscg)
Performance Calculations	Cross-Entropy (crossentropy) MEX

The input matrix **thrusterInputs\_RWE** has been randomly divided up into training samples (70%), Validation samples (15%) and Testing samples (15%). These samples were presented to the network during training, and the network was adjusted according to its error. Validation samples were used to measure network generalization, and to halt training when the generalization stops improving. The testing samples have no effect on training and provide an independent measure of network performance during and after training. The training, Validation and Confusion Matrices are shown in Figure 9. On the confusion matrix plot, the rows correspond to the predicted class (Output Class), and the columns show the true class (Target Class). The diagonal cells show for how many (and what percentage) of the examples the trained network correctly estimates the classes of observations. That is, it shows what percentage of the true and predicted classes match. The off diagonal cells show where the classifier has made mistakes. The column on the far right of the plot presents the accuracy for each predicted class, while the row at the bottom of the plot shows the accuracy for each true class. The cell in the bottom right of the plot shows the overall accuracy.

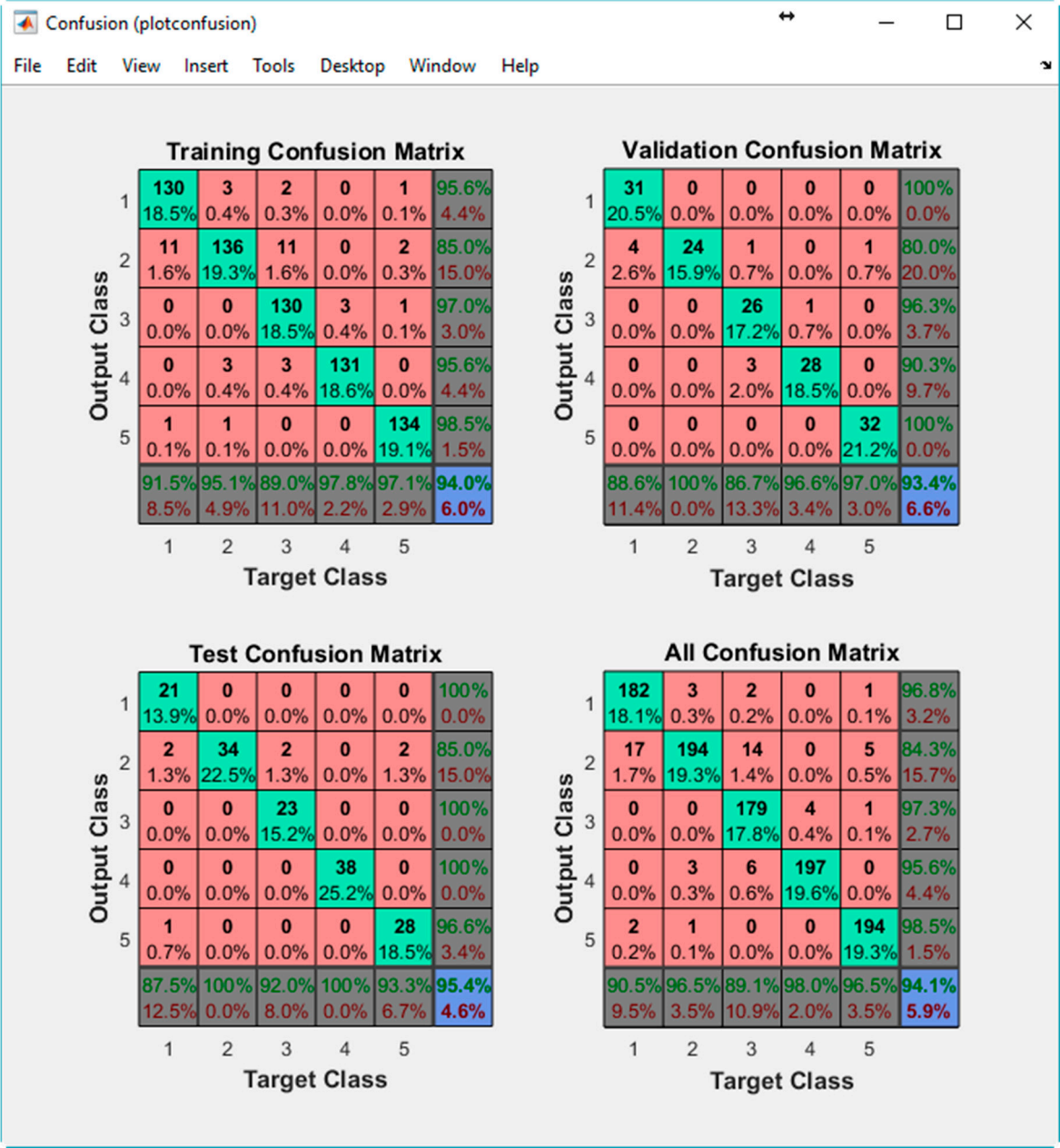


Figure 9. Plots of Training, Validation, Test and All Confusion Matrices.

Figure 10 displays the Neural Network Cross-Entropy and Performance plots. Minimizing Cross-Entropy within the neural network results in enhanced classification.

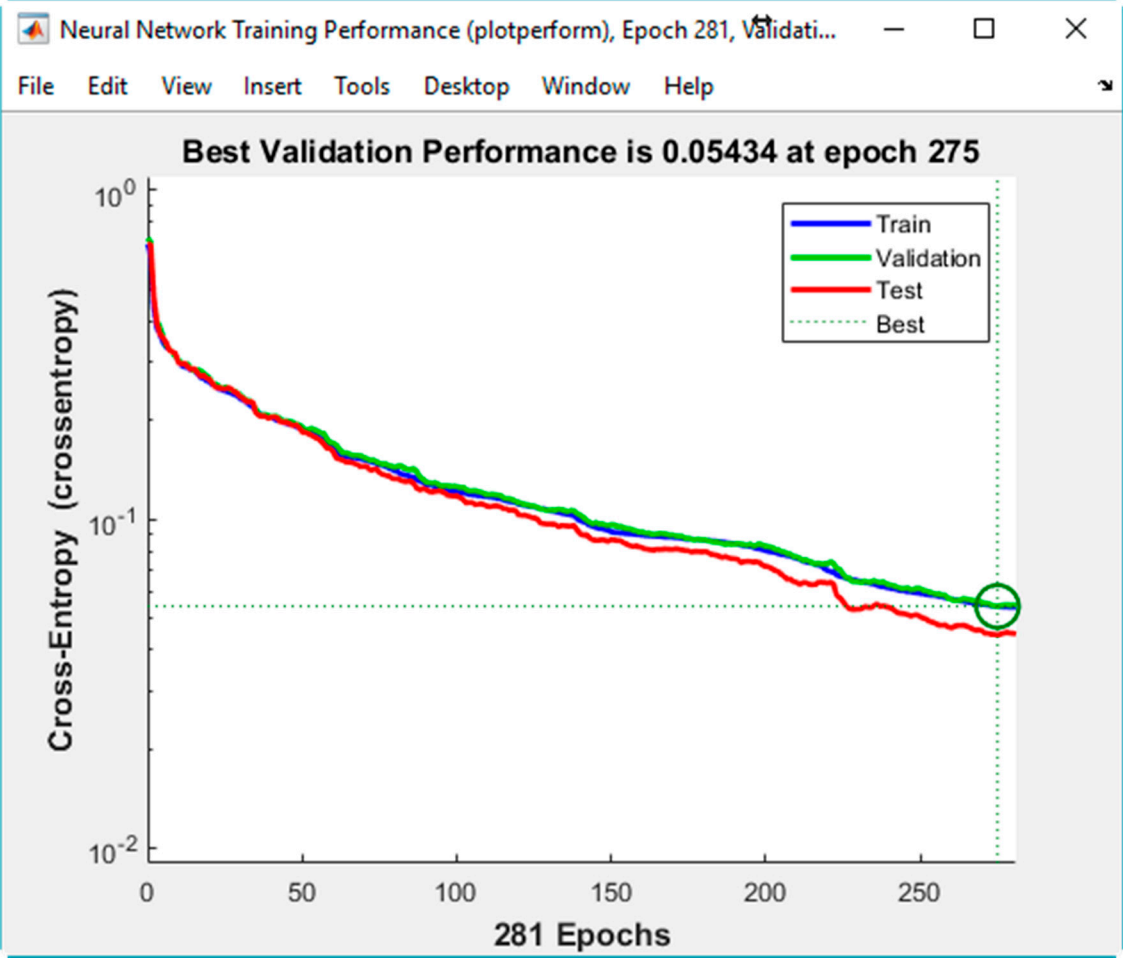


Figure 10. Neural Network Cross-Entropy and Performance plots.

The Receiver Operating Characteristic (ROC) is a metric employed to check the quality of classifiers. For each class of a classifier, the ROC applies threshold values across the interval  $[0,1]$  to outputs. For each threshold, two values are calculated, the True Positive Ratio (TPR) and the False Positive Ratio (FPR). For a particular class  $i$ , the TPR is the number of outputs whose actual and predicted class is class  $i$ , divided by the number of outputs whose predicted class is class  $i$ . The FPR is the number of outputs whose actual class is not class  $i$ , but predicted class is class  $i$ , divided by the number of outputs whose predicted class is not class  $i$ . Figure 11 displays the ROC for each output class of PRNN. The more each curve hugs the left and top edges of the plot, the better the classification.

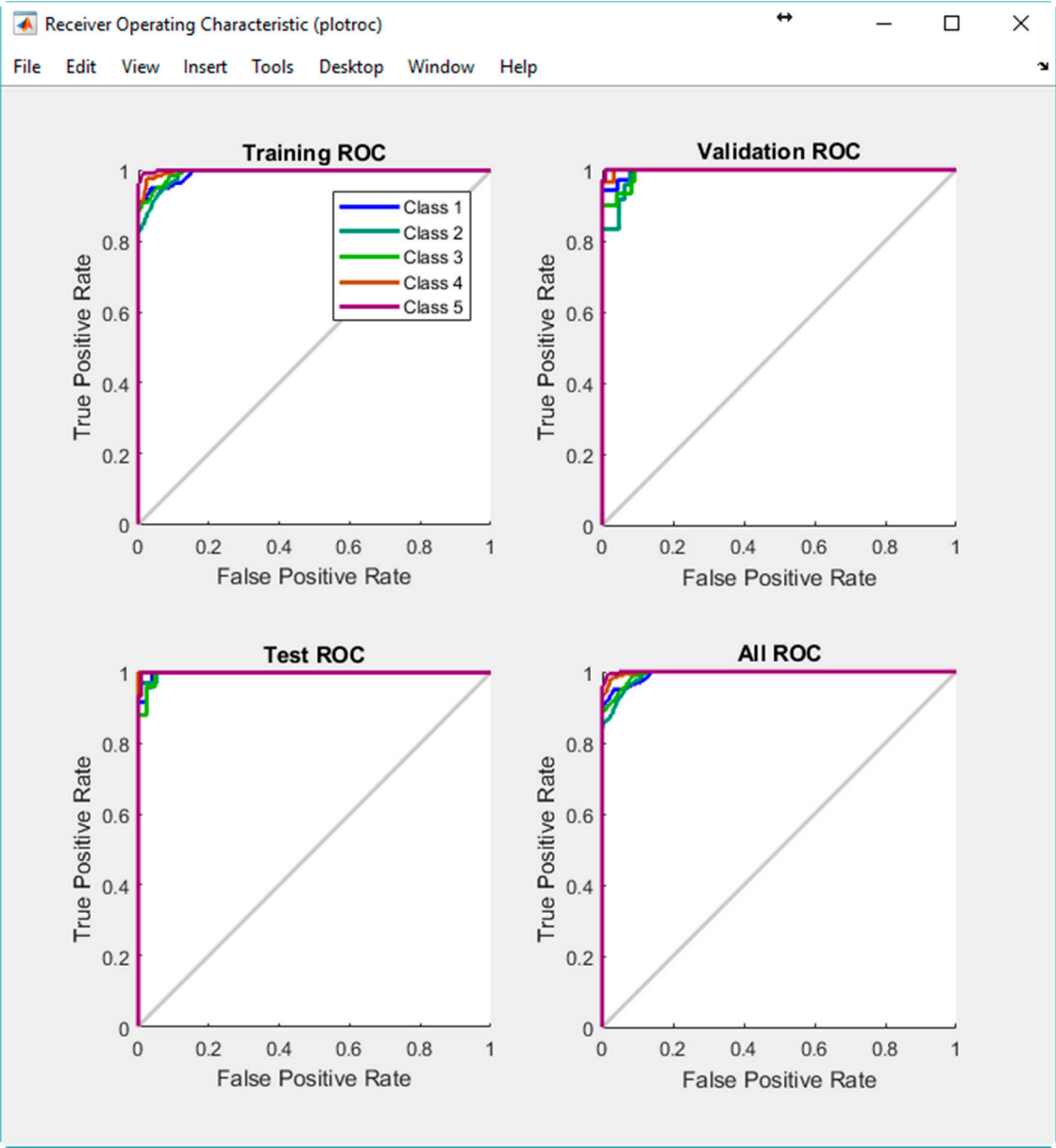


Figure 11. Receiver Operating Characteristic plots.

The classification performance of the PRNN in the real-world environment is verified in section 4.

In the *third* and last stage of the training phase, the structure of the trained PRNN is saved as a MATLAB function `nn_pr_16_RWE` on the hard disk for future use. In this way, time consuming training calculations are performed off-line, during the training phase, which enables fast and efficient detection during the on-line phase.

On-line fault detection phase

From the preceding discussion, the problem of thruster fault detection is considered as a pattern recognition problem. An original method for on-line fault detection, adapted to the specific features of the underlying pattern recognition problem, will now be described.

During the initialisation stage of the on-line fault detection phase, training data for each class (acquired in the off-line training phase) are loaded into memory and displayed as separate static background plots  $I$  versus  $n_d$  and  $n$  versus  $n_d$  for each layer (HT Layer 0, HT Layer 1 and VT Layer). These plots are utilised to represent the relationship between variables for different thruster states and for visualisation of actual thruster measurements in real-time. Additional activities during initialisation phase include memory allocation for buffers, reading fault code table settings from file and the creation of action lists.



After the initialisation is finished, the fault detection is performed by repeating the steps from the FDU Algorithm (Table 9) for each thruster at each programme cycle:

Table 9. FDU Algorithm – On-line fault detection.

FDU Algorithm	
1.	Read values for external faults ( $n_d$ , $I$ and $n$ ) and internal faults ( $V$ and $T$ ) from TCU.
2.	Create vector $x = [n_d \ I \ n]^T$ and execute $y = \text{nn\_pr\_16\_RWE}(x)$ ; $y = \text{round}(y)$ ; <sup>1</sup>
3.	Combine fault code table (Table 3) and thruster target table (Table 6) to determine thruster external fault state and corresponding actions A & B.
4.	Determine internal fault state and actions A & B from thruster fault code table by examining if values of $V$ and $T$ exceed the limits.
5.	(Optional) Use prioritisation scheme to resolve simultaneous appearance of external and internal faults: total faults have higher priority than partial faults.
6.	Deliver the final thruster state and actions A & B as output.

<sup>1</sup> Vector  $y$  will have one of the following six values:  $[1;0;0;0;0]$ ,  $[0;1;0;0;0]$ ,  $[0;0;1;0;0]$ ,  $[0;0;0;1;0]$ ,  $[0;0;0;0;1]$ ,  $[0;0;0;0;0]$ . The last value is obtained in cases when a thruster operates in an unknown regime i.e. out-of-normal regime, different from faulty cases shown in Table 5. Typical examples for this case from the real-world environment include propeller jammed with rope or seaweed. The thruster state associated with value  $y = [0;0;0;0;0]$  is "Unknown" (see Thruster Fault Code Table in Table 3).

It should be mentioned that, in order to avoid false detection due to outliers and measurement noise, the outputs of FDU Algorithm are buffered i.e. the final decision about thruster fault is not derived from a single measurement, but is accomplished using present and past thruster states (FDU Algorithm outputs), which are stored in the buffer. This buffer operates similar to the shift register: when the new state is pushed into the buffer, the other states are pushed (shifted) down and the "oldest" state is pushed (shifted) out. Elements of the buffer are compared to each other, and if all buffer elements have the same value (state), then the aggregate thruster state is set to this value. Otherwise, the previous value is kept as the aggregate state.

3.3. FA subsystem

The proposed FA subsystem is an extension of the hybrid approach for control allocation based on integration of the pseudoinverse and the fixed-point iteration method which compensates the thruster fault effect [13,14]. It is implemented as a two-step process. The pseudoinverse solution is found in the first step. Then the feasibility of the solution is examined, analysing its individual components. If violation of actuator constraint(s) is detected, the fixed-point iteration method is activated in the second step. In this way, the hybrid approach is able to allocate the exact solution, optimal in the  $l_2$  sense, inside the entire attainable command set. This solution minimises a control energy cost function, the most suitable criteria for underwater applications.

As stated in section 3.1, the HT Synthesis and VT Synthesis modules create virtual control vectors  $\tau_{HT}$  and  $\tau_{VT}$ . These vectors represent the total control effort (normalised forces and moments) to be produced by the actuators (thrusters). Control Allocators in Figure 2 find individual actuator settings (true control vectors  $u_{HT}$  and  $u_{VT}$  for horizontal and vertical thrusters, respectively) to be applied in order to produce desired control effort. The Fault Accommodation (FA) subsystem uses FDI outputs (aggregate thruster states) and associated software-level actions (action A) and hardware-level actions (action B) to solve the control allocation problem for each thruster layer in presence of partial/total thruster faults. Action A (see Table 3) includes penalisation of faulty thruster in the solution of control allocation problem by restricting saturation bounds i.e. by increasing the corresponding weight in the weighting matrix [14]. Action B includes power isolation of faulty thrusters (total faults only in Table 3) such that the entire ROV power system is not compromised. Hence, if the aggregated thruster state is a partial fault, the thruster is penalised, but will continue to operate. However, in the case of a total fault, the thruster is removed from the control allocation process, and its power is switched off in parallel.

3.4. Software Implementation

The proposed FTC has been implemented as a LabVIEW VI named “Thruster Active FDI”, which is a software module integrated with other OceanRINGS+ modules. The user interface, which shows FDI results, is presented in Figure 12. This image is just an example; it has been artificially generated by injecting faults in the simulated thruster models, and it is intended to illustrate various options available in the software to detect, isolate and accommodate faults. The display is divided into 3 groups: horizontal thrusters (Layer 0 & Layer 1) and vertical thrusters. Each state has an associated colour code box. The external faults are represented with a column named “States”, while internal faults are displayed as columns named “Voltages” and “Temperatures”. The fault code table for the individual layers can be edited on the configuration tab of the main application. The fault code table for the horizontal thrusters (Layer 0) can be viewed in Figure 13.

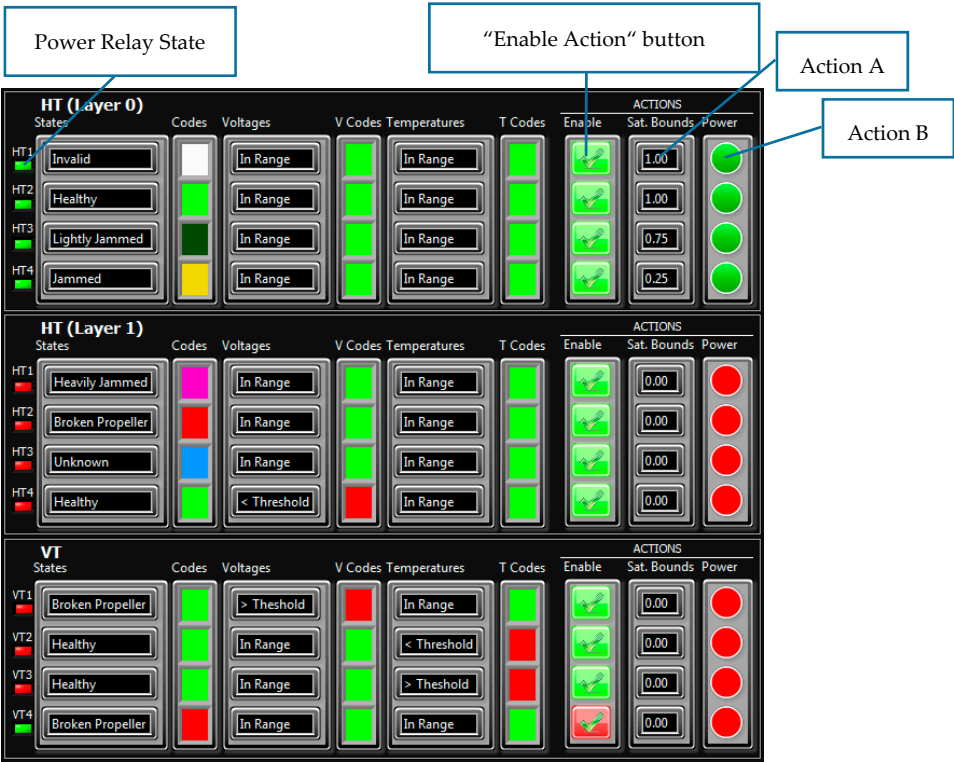


Figure 12. User Interface showing thruster FDI states and actions.



Figure 13. Fault Code Table for horizontal thrusters (Layer 0).

In order to increase the flexibility of the proposed FTC scheme, each thruster has associated individual “Enable Action” buttons. If the “Enable Action” is true, actions A & B will be applied. If the “Enable Action” is false, no actions will be applied i.e. the FDI subsystem will detect fault, but no action will be executed by the FA subsystem.

Thrusters HT1, HT2, HT3 & HT4 in Layer 0 in Figure 12 have “Enable Action” buttons set to true. The FDI subsystem has detected external faults (partial faults) in HT3 (Lightly Jammed) and HT4 (Jammed) and no presence of internal faults. All four thrusters remain powered on, while the software-level actions resulted in Saturation Bounds set to 0.75 and 0.25 for HT3 and HT4, respectively.

In a similar way, thrusters HT1, HT2, HT3 & HT4 in Layer 1 in Figure 12 have “Enable Action” buttons set to true. In this case, the FDI has detected external faults (total faults) in HT1 (Heavily Jammed), HT2 (Broken) and HT3 (Unknown), and presence of an internal fault in HT4 (Voltage < Threshold). Hardware-level actions resulted that the power to all four thrusters is switched off (as was confirmed by the power relay states for HT1-HT4, Layer 1), while software-level actions resulted in Saturation Bounds set to 0 for all four thrusters.

Finally, thrusters VT1, VT2 & VT3 have “Enable Action” buttons set to true. The FDI has detected external fault (total fault) in VT1 (Broken Propeller), and internal faults (total faults) in VT2 (Temperature < Threshold) and VT3 (Temperature > Threshold). Hardware-level actions resulted that the power to all three thrusters is switched off (as confirmed by Power Relay States), while software-level actions resulted in Saturation Bounds set to 0 for all three thrusters. Thruster VT4 has “Enable Action” button set to false. The FDI has detected an external fault (total fault) in VT4 (Broken Propeller) and no presence of internal faults. However, the FA subsystem did not execute action A (set Saturation Bounds to 0) and action B (switch off power to the thruster, as confirmed with power relay state for VT4).

An event log table is used to log Fault Detection and Isolation (FDI) events i.e. details of thruster external and internal faults as they occur. The FDI Event Log Table data includes event I.D., date and timestamp of fault occurrence, thruster in which fault occurred, type of external and internal fault

and, if the “Enable Action” button is set to `true`, the software-level and hardware-level actions that were applied. An example of the FDI Event Log Table is shown in Figure 14.

FDI Event Log								
ID	Date	Time	Thruster	State	Voltage	Temperature	Action (S)	Action (H)
0014	22/01/2018	12:06:45	VT4	Lightly Jammed	In Range	In Range	NONE	NONE
0013	22/01/2018	12:06:34	VT4	Lightly Jammed	In Range	In Range	NONE	NONE

Figure 14. Thruster Fault Detection and Isolation (FDI) Event Log table.

4. Testing and Evaluation of the FTC

The performance of the FTC, proposed and described in section 3, is evaluated and tested in a real-world and virtual (simulated) environment. In the real-world environment, a single M5 VideoRay thruster has been utilised to evaluate the FTC performance for various fault conditions. In the virtual (simulated) environment, various thruster fault conditions were simulated in order to examine the behaviour of the FTC in different situations (open-loop/closed-loop control performance with enabled/disabled FA actions).

4.1. Evaluation of the FTC in real-world environment

A single M5 VideoRay thruster, configured as VT4, has been used for post-training validation of the trained PRNN and to evaluate the performance of the FTC in fault-free mode (no object attached to the propeller) and faulty modes (with “blockages” of various sizes and shapes attached to the blades, see Figure 4). The main objective was to evaluate the capability of the FDI subsystem to detect thruster states for external faults only, with a disabled FA subsystem (the “Enable Action” button set to `false` for VT4). The thruster was actuated with the same signal that has been used to acquire training data (Figure 15) i.e. with saw-like command signal  $n_d$  (%) with the following pattern:  $0\% \gg \text{MAX}\% \gg 0\% \gg -\text{MAX}\% \gg 0\%$ , step size 1%. The total duration of signal was  $T = 20$  seconds, sampling period  $50\text{ ms}$  and max. value  $\text{MAX} = 100\%$ . The critical (forbidden) zone has been set to  $n_d \in [-20\%, 20\%]$ . Screenshots of the FDI results for various thruster states are shown in Figures 16 – 20. Note that the results are for VT4 only. All other thruster states are shown as Invalid.

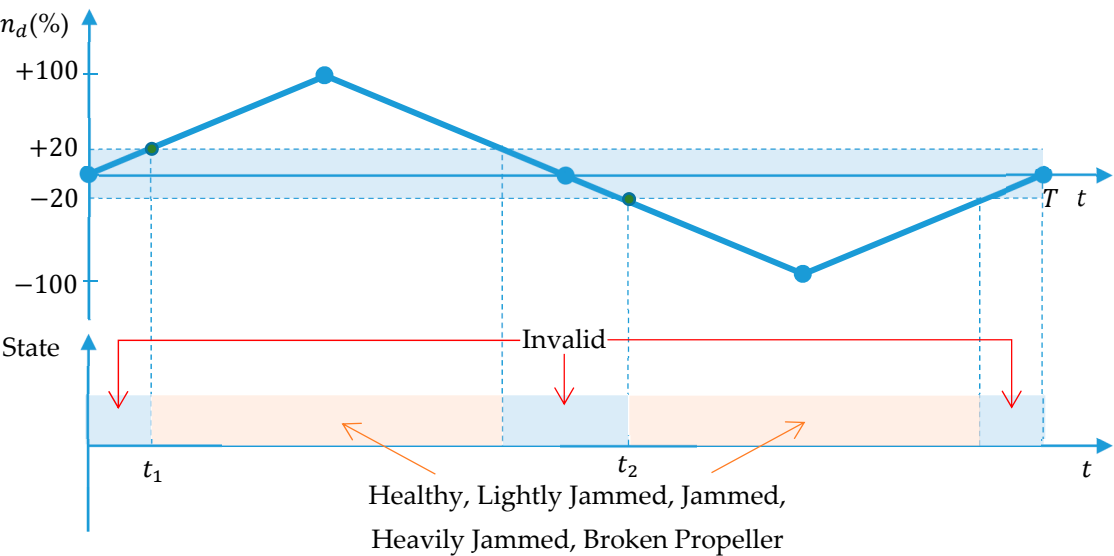


Figure 15. Time responses of command signal and thruster states.





Figure 16. Thruster FDI result for thruster state = "Healthy".



Figure 17. Thruster FDI result for thruster state = "Lightly Jammed".



Figure 18. Thruster FDI result for thruster state = "Jammed".



Figure 19. Thruster FDI result for thruster state = "Heavily Jammed".

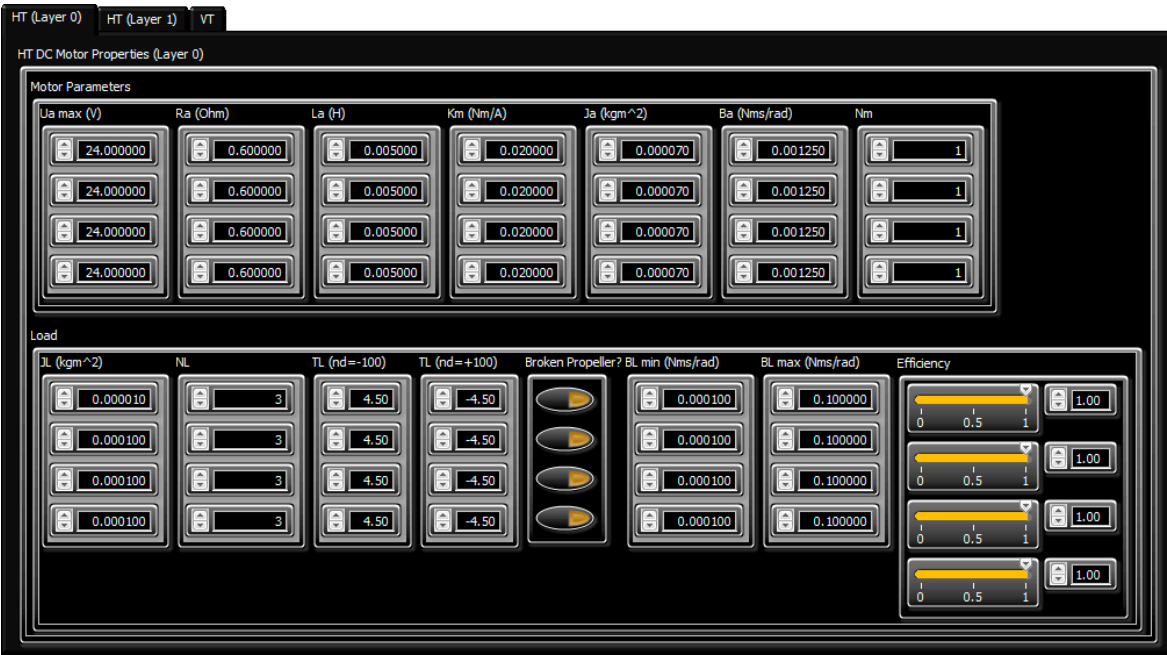


Figure 20. Thruster FDI result for thruster state = “Broken Propeller”.

The FDI subsystem registers events only when the command signal  $n_d$  leaves the critical (forbidden) zone. Two events have been logged for each fault: the Event 1 with timestamp  $t_1$  (time instance when the command signal  $n_d$  left the critical zone for the first time, see Figure 15), and the Event 2 with timestamp  $t_2$  (time instance when the command signal  $n_d$  left the forbidden zone for the second time). While passing through the forbidden zone, the FDI subsystem went to “sleep” mode indicating a thruster state = “Invalid”. The PRNN correctly recognised a thruster state outside the forbidden zone in all five cases. Test results confirmed that the PRNN has 100% classification accuracy outside the forbidden zone, and that the miss-classification appears exclusively inside the critical (forbidden) zone, as predicted in section 3.1.

4.2. Evaluation of the FTC in virtual (simulated) environment

As mentioned in section 3.2, in the virtual (simulated) environment thruster faults are simulated by varying properties of the thruster dynamic model (load, friction, etc.) inside the propulsion subsystem of the ROV dynamics simulator. Off-line training and on-line fault detection phases are performed in the same way as described in section 3.2 for the real-time environment but, in this case, faults are simulated by varying efficiency of thruster or by pushing the “Broken Propeller” button on the Thruster Configuration tab, shown in Figure 21.



**Figure 21.** Thruster Configuration tab for horizontal thrusters (Layer 0) in the ROV dynamics simulator.

A description of the simulation test cases, presented in this section, is given in Table 10.

**Table 10.** Description of simulation tests.

ID	Type	LLC Settings	Thruster	Fault	“Enable Action”
1	Open-Loop $\tau_x(VJ) = 0.3$ $\tau_y(VJ) = 0.0$ $\tau_z(VJ) = 0.0$	Heading: OFF Surge Speed: OFF Sway Speed: OFF	HT2 (L0)	Broken Propeller	False
2	Closed-Loop $SOG_d = 0.54m/s$ $COG_d = 60^\circ$	$Y_d = COG_d$ $u_d = proj(SOG_d)_x$ $v_d = proj(SOG_d)_y$	HT2 (L0)	Broken Propeller	False
3	Closed-Loop $SOG_d = 0.54m/s$ $COG_d = 60^\circ$	$Y_d = COG_d$ $u_d = proj(SOG_d)_x$ $v_d = proj(SOG_d)_y$	HT2 (L0)	Broken Propeller	True

The test cases described in Table 10 enable investigation of the influence of thruster faults on the overall control performance of the ROV and demonstrate the ability of the FTC to accommodate the faults and minimise the negative impact on control performance. It should be emphasized that similar test cases have been conducted with total and partial faults in vertical thrusters, and the main conclusion is that the ROV control system with active FDI and FA subsystems is capable of maintaining full 3 DOF in the vertical plane in the presence of a partial or total fault in a single vertical thruster.

Test 1: Impact of “Broken Propeller” in Open-Loop mode with disabled fault accommodation

In this case, the Surge, the Sway and the Yaw LLCs are disabled and the virtual control vector  $\tau_{HT} = [0.3 \ 0.0 \ 0.0]^T$  is constant during the duration of the test. At time instance  $t_0$  the “Broken Propeller” fault occurs in HT2, Layer 0. The FDI subsystem detects the fault and logs the FDI event, but the FA subsystem does not perform any action, since the “Enable Action” button is set to false (Figure 22). For this reason, the Control Allocator still assumes that the thruster HT2 is healthy and does not modify the solution of the control allocation problem. However, since HT2 does not



produce any thrust/moment, the ROV drifts to the right side, with continuous change in heading (Figure 23).

Test 2: Impact of “Broken Propeller” in Closed-Loop mode with disabled fault accommodation

In this case, the Surge, the Sway and the Yaw LLCs are enabled, while all components of the Virtual Joystick vector are set to zero. The Speed Mode is set to SM2 (Follow Speed and Course) and the Heading Mode is set to HM2 (Follow Course). The Desired Speed Over Ground ( $SOG_d$ ) is set to  $0.54\text{m/s}$ , and Desired Course Over Ground ( $COG_d$ ) is set to  $60^\circ$ . The set points  $u_d$  for Surge Speed LLC and  $v_d$  for Sway Speed LLC are found as projections of the velocity vector in the horizontal plane on the  $x$  and  $y$  axis of the body-fixed  $\{b\}$  frame. At time instance  $t_0$  the “Broken Propeller” fault occurs in HT2, Layer 0. The FDI subsystem detects the fault and logs the FDI event, but the FA subsystem does not perform any action, since the “Enable Action” button is set to `false` (Figure 24). Similar to Test 1, the Control Allocator still assumes that the thruster HT2 is healthy. However, robustness of closed-loop low-level controllers limit the ROV drift to the starboard side with a heading offset of  $4.833^\circ$  (Figure 25).

Test 3: Impact of “Broken Propeller” in Closed-Loop mode with enabled fault accommodation

Similar to Test 2, the Surge, the Sway and the Yaw LLCs are enabled, all components of Virtual Joystick vector are set to zero, the Speed Mode is set to SM2 (Follow Speed and Course) and the Heading Mode is set to HM2 (Follow Course). At time instance  $t_0$  the “Broken Propeller” fault occurs in HT2, Layer 0. Since the “Enable Action” button is set to `true` (Figure 26), the FDI subsystem detects the fault and logs the FDI event, and the FA subsystem sets Saturation Bounds to zero for HT2 (action A) and switches off the thruster power (action B). The Control Allocator penalises (excludes) the faulty thruster in the solution of the control allocation problem and reallocates control energy among the operable thrusters (Figure 27). Small changes in the surge & sway speeds and heading are visible during the transient stage. The appearance of these transients is unavoidable, since operable thrusters need time to spin to new setpoints. However, after a short time period, all these changes diminish and the ROV continues in a straight-line motion, following the desired speed and course without error (Figure 27).

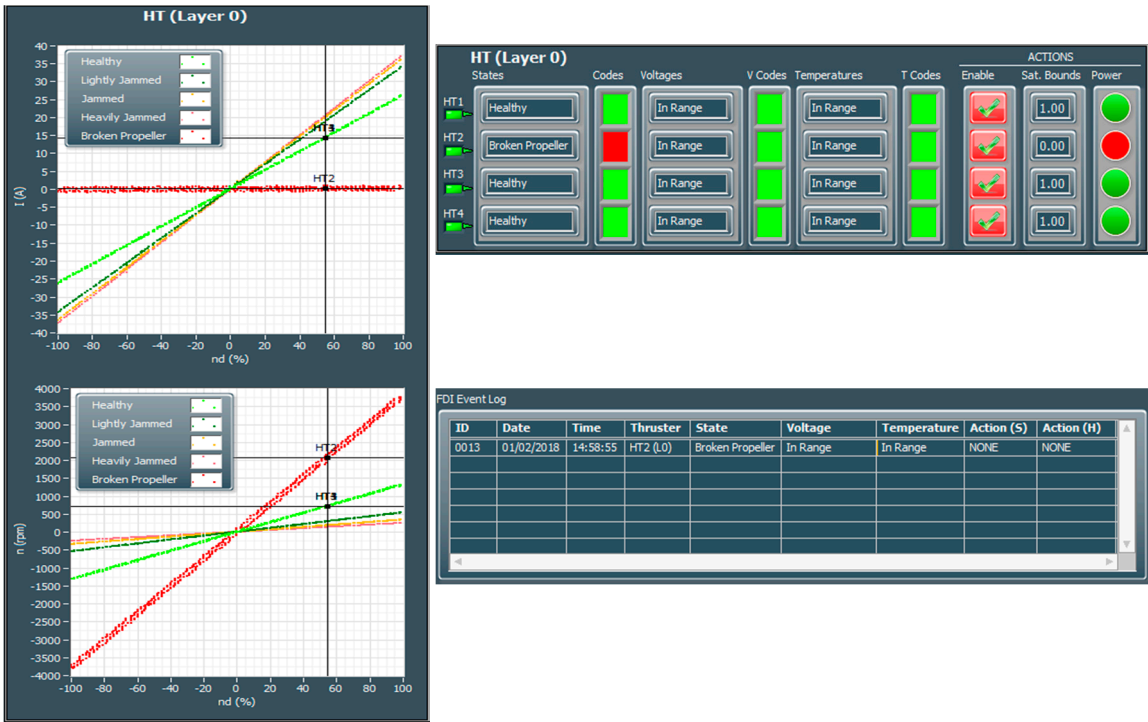
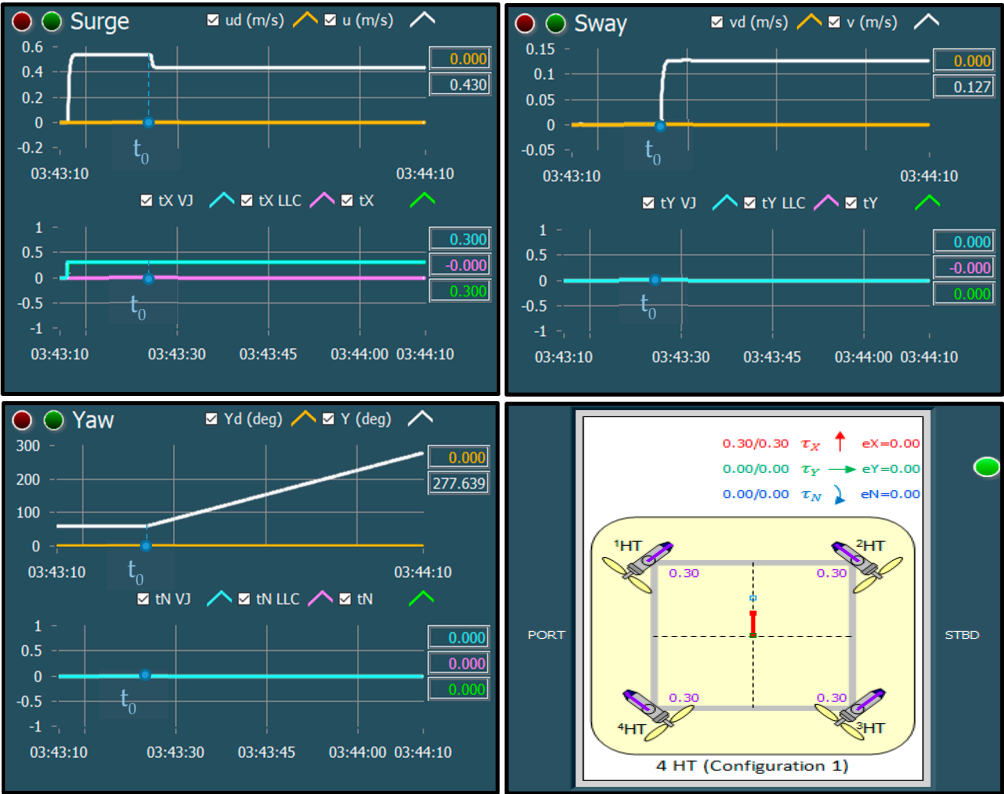


Figure 22. Test 1 (Open-Loop): Total fault in HT2 (“Broken Propeller”) with disabled fault accommodation.



**Figure 23.** Test 1 (Open-Loop): Total fault in HT2 (“Broken Propeller”) occurred at  $t_0$ ; the lack of fault accommodation causes the ROV to drift with continuous change in heading.



**Figure 24.** Test 2 (Closed-Loop): Total fault in HT2 (“Broken Propeller”) with disabled fault accommodation.

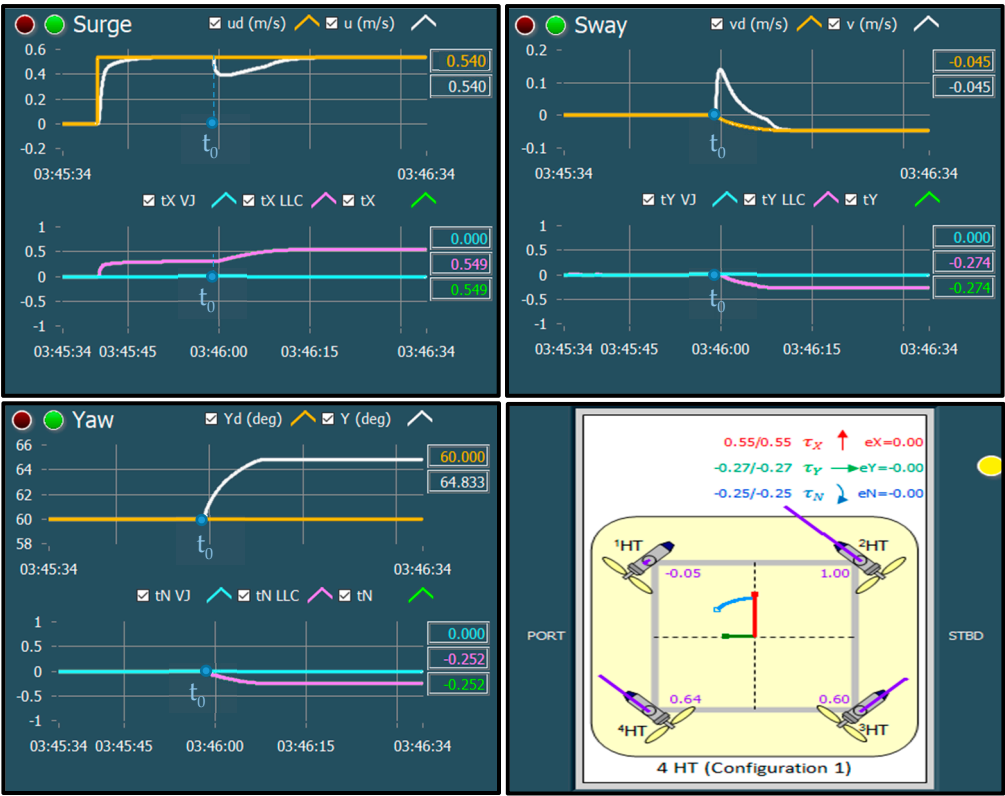


**Figure 25.** Test 2 (Closed-Loop): Total fault in HT2 (“Broken Propeller”) occurred at  $t_0$ ; the lack of fault accommodation and robustness of the closed-loop controllers causes limited drift to the starboard side with a heading offset of 4.833°.



**Figure 26.** Test 3 (Closed-Loop): Total fault in HT2 (“Broken Propeller”) with enabled fault accommodation.

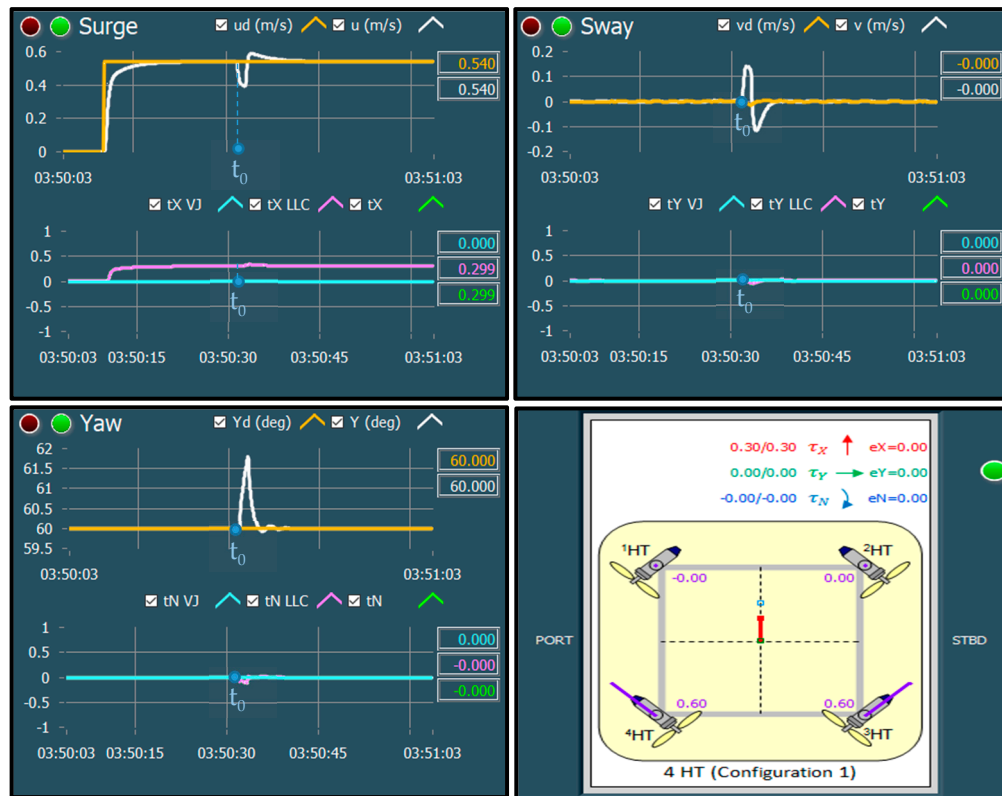


**Figure 27.** Test 3 (Closed-Loop): Total fault in HT2 ("Broken Propeller") occurred at  $t_0$ ; excellent control performance is achieved due to fault accommodation and robustness of closed-loop controllers.

## 5. Conclusions and Future Work

This paper described a novel thruster fault-tolerant control system (FTC) for open-frame remotely operated vehicles (ROVs), developed by researchers at the Centre for Robotics & Intelligent Systems (CRIS), University of Limerick. The proposed FTC system is part of the OceanRINGS+ ROV smart control system, currently under development.

The proposed FTC consists of two subsystems: a model-free thruster fault detection and isolation subsystem (FDI) and a fault accommodation subsystem (FA). The FDI subsystem employs fault detection units (FDUs), associated with each thruster, to monitor their state. The robust, reliable and adaptive FDUs use a model-free pattern recognition neural network (PRNN) to detect internal and external faulty states of thrusters in real time. The FA subsystem combines information provided by the FDI subsystem with predefined, user-configurable actions to accommodate partial and total faults and to perform an appropriate control reallocation. Software-level actions include penalisation of faulty thrusters in solution of the control allocation problem and reallocation of control energy among the operable thrusters. Hardware-level actions include power isolation of faulty thrusters (total faults only) such that the entire ROV power system is not compromised.

Using simulations and real-world tests, the performance of the FTC was evaluated through a series of representative test cases, in order to examine the behaviour of the FTC in fault-free and faulty conditions. In the real-world environment, a single M5 VideoRay thruster has been used to evaluate the FTC performance for various fault conditions. Test results confirmed that the PRNN has 100% classification accuracy outside the forbidden zone, and that the miss-classification appears exclusively inside the critical (forbidden) zone. In the virtual (simulated) environment, various thruster fault conditions were simulated in order to examine the behaviour of the FTC in different situations (open-loop/closed-loop control performance with enabled/disabled FA actions). Simulation results show that the FTC provides automatic reallocation in faulty conditions, keeping all the DOF in the horizontal plane fully controllable and providing the opportunity to continue the mission with a minimal loss of control performance.

In the worst case scenario, the proposed FTC is able to maintain full 6 DOF control of the ROV in presence of up to 6 simultaneous total faults in thrusters (one layer with four horizontal thrusters fully disabled plus one disabled thruster in the other layer of horizontal thrusters plus one disabled vertical thruster).

Future work includes extension of the proposed FTC to interface with other ROVs and development of a “passive” method for fault detection and isolation for ROVs with thrusters that cannot provide active real-time monitoring of relevant signals from thrusters (currents, shaft speeds, applied voltages and temperatures of windings).

**Acknowledgments:** This paper is based upon works supported by the Science Foundation Ireland under Grant No. 12/RC/2302 for the Marine Renewable and Energy Ireland (MaREI) centre. SFI funding has been in collaboration with industry partners IDS Monitoring, Shannon Foynes Port Company, Commissioners of Irish Lights and Teledyne BlueView.

**Author Contributions:** R.C. and E.O. wrote the paper. R.C. designed the hardware and software for the FDI and constructed the test rig for the real-world tests, under E.O. supervision. G.D. provided guidance in the selection of hardware for the system. G.D. and D.T. proof read and provided guidance on the correct structure of the paper.

**Conflicts of Interest:** The authors declare no conflict of interest. The founding sponsors had no role in the design of the study; in the collection, analyses, or interpretation of data; in the writing of the manuscript, and in the decision to publish the results.

## References

- Capocci, R.; Dooly, G.; Omerdić, E.; Coleman, J.; Newe, T.; Toal, D. Inspection-class remotely operated vehicles-a review. *J. Mar. Sci. Eng.* **2017**, *5*.
- O'Connor, M.; Lewis, T.; Dalton, G. Weather window analysis of Irish west coast wave data with relevance to operations & maintenance of marine renewables. *Renew. Energy* **2013**, *52*, 57–66.
- Yusoff, M. A. M.; Arshad, M. R. Active Fault Tolerant Control of a Remotely Operated Vehicle Propulsion System. *Procedia Eng.* **2012**, *41*, 622–628.
- Baldini, A.; Ciabatonni, L.; Felicetti, R.; Ferracuti, F.; Monteriù, A.; Fasano, A.; Freddi, A. Active fault tolerant control of remotely operated vehicles via control effort redistribution. In *Proceedings of the ASME Design Engineering Technical Conference; 2017; Vol. 9*, pp. 1–7.
- Antonelli, G. A Survey of Fault Detection/Tolerance Strategies for AUVs and ROVs. In *Fault Diagnosis and Fault Tolerance for Mechatronic Systems: Recent Advances*; Caccavale, F.; Villani, L., Eds.; Springer Berlin Heidelberg: Berlin, Heidelberg, 2003; pp. 109–127.
- Soylu, S.; Buckham, B. J.; Podhorodeski, R. P. A chattering-free sliding-mode controller for underwater vehicles with fault-tolerant infinity-norm thrust allocation. *Ocean Eng.* **2008**, *35*, 1647–1659.
- Hanai, A. M.; Choi, S. K.; Marani, G.; Rosa, K. H. for Underwater Vehicles. In *2009 IEEE International Conference on Robotics and Automation*; Kobe, Japan, 2009; pp. 194–199.
- Corradini, M. L.; Orlando, G. A Robust Observer-Based Fault Tolerant Control Scheme for Underwater Vehicles. *J. Dyn. Syst. Meas. Control* **2014**, *136*, 34504.
- Zhu, D.; Liu, Q.; Hu, Z. Fault-tolerant control algorithm of the manned submarine with multi-thruster based on quantum-behaved particle swarm optimisation. *Int. J. Control* **2011**, *84*, 1817–1829.
- Caccia, M.; Bono, R.; Bruzzone, G.; Bruzzone, G.; Spirandelli, E.; Veruggio, G. Experiences on Actuator Fault Detection, Diagnosis and Accommodation for ROVs. In *International Symposium Unmanned Untethered Submersible Technology*; Durham, New Hampshire, 2001.
- Zhao, B.; Skjetne, R.; Blanke, M.; Dukan, F. Particle Filter for Fault Diagnosis and Robust Navigation of Underwater Robot. *IEEE Trans. Control Syst. Technol.* **2014**, *22*, 2399–2407.
- Omerdic, E.; Toal, D.; Dooly, G. OceanRINGS: Smart Technologies for Subsea Operations. Chapter in book “Advanced in Marine Robotics”, Lambert Academic Publishing, ISBN-13: 978-3-659-41689-7, ISBN-10: 3659416894.
- Omerdic, E.; Toal, D.; Nolan, S.; Ahmad, H. ROV LATIS: Next Generation Smart Underwater Vehicle. Chapter 2 in the IET Book: Further Advances in Unmanned Marine Vehicles, ISBN-10: 1849194793, ISBN-13: 9781849194792, Publisher: Inst of Engineering & Technology.



- 667 14. Omerdic, E.; Roberts, G. Extension of Feasible Region of Control Allocation for Open-frame Underwater  
668 Vehicles. IFAC Conference on Control Applications in Marine Systems (CAMS 2004), Ancona, Italy.
- 669 15. Omerdic, E.; Roberts, G. Thruster fault diagnosis and accommodation for open-frame underwater  
670 vehicles. *Control Eng. Pract.* **2004**, *12*, 1575–1598.
- 671 16. Omerdic, E.; Toal, D.; Nolan, S.; Ahmad, H. Smart ROV LATIS: Control Architecture. UKACC  
672 International Conference on CONTROL 2010, Coventry, UK, 7th-10th September 2010.